Co-deformation and dynamic annealing effects on the texture development during alpha–beta processing of a model Zr-Nb alloy

Christopher S. Daniel[1*], Alistair Garner[2], Peter D. Honniball[3], Luke Bradley[3], Michael Preuss[2], Philip B. Prangnell[1], João Quinta da Fonseca[1]

[*]Corresponding author, email: christopher.daniel@manchester.ac.uk

[1]Centre for Light Alloy Research and Innovation, The University of Manchester, Manchester, M13 9PL, UK

[2]Materials Performance Centre, The University of Manchester, Manchester, M13 9PL, UK

[3]Rolls-Royce plc, Derby, DE21 7XX, UK

Keywords: alpha-beta processing, zirconium alloys, titanium alloys, crystallographic texture, 3D EBSD

Abstract

The in-service properties and performance of dual-phase Zr and Ti alloys depend on their crystallographic texture, which develops during hot-working and is affected by interactions between the α and β phases during deformation, annealing and phase transformation. Recent work on hot-rolled Zr-2.5Nb has shown that the texture of the two phases are related, with coupled strengthening of the α near $\{11\bar{2}0\}\langle 10\bar{1}0\rangle$, which produces strong 0002 pole intensities along the transverse direction, and β with $\{001\}\langle 110\rangle$ rotated cube, particularly when the relative volume fraction is around 50:50. To investigate the origin of this texture coupling, we studied a hot-rolled model Zr alloy with 7 wt.% Nb, in which the as-deformed α + β microstructure is preserved on cooling. The alloy was hot-rolled to different reductions at 725°C, which corresponds to a relative α:β volume fraction of 30:70, where the characteristic textures are known to develop quickly at first and then weaken with further reduction. The rolled material was characterised using both 2D and 3D electron backscatter diffraction (EBSD). This analysis uncovered evidence that both recrystallization and phase transformation cause the disappearance of specific α variants during rolling, favouring the formation of "soft" primary α grains flattened in $\langle 11\bar{2}0\rangle$ and elongated along $\langle 10\bar{1}0\rangle$ during rolling, which in turn has an effect on surrounding β orientations, promoting the stronger rotated cube

component. At higher reductions, these elongated α-grains start to break up, as does the β surrounding it, forming bands of characteristic coupled textures. These observations imply that non-plasticity effects should be included in models of texture evolution during processing of α + β Zr and Ti alloys.

1 Introduction

Dual-phase α + β Zr and Ti alloys develop strong crystallographic textures during processing, which strongly influence the performance of nuclear [1] and aerospace [2] components. The thermomechanical processing of these alloys is carried out at elevated temperatures and therefore phase transformation and annealing will occur during heating, deformation and cooling, all of which can contribute to the texture development. Unravelling the complex interactions between these different mechanisms and determining their relative contribution is difficult, even more so because the β-phase, which makes up over half of the material during deformation, transforms to secondary α on cooling, obscuring important details of its deformed state.

Zr-2.5Nb and Ti-6Al-4V (Ti-64) alloys are usually hot worked via α + β forging, extrusion [3–5] or rolling [2,6–10]. The characteristic α-texture that develops is a strong transverse (TD) alignment of the 0002 basal poles [2,6–10], and alignment of the prismatic $10\bar{1}0$ poles along RD (ED for extrusion), and therefore the main texture component is near $\{11\bar{2}0\}\langle 10\bar{1}0\rangle$ (often also referred to as 0002||TD). In some cases, the 0002 pole deviates from TD, and the dominant component becomes $\{11\bar{2}1\}\langle 10\bar{1}0\rangle$ [6,9].

During hot-rolling, the texture strength depends on the processing temperature and is strongest when both phases are present in similar volume fractions [6,8]. At lower temperatures and high α volume fractions (< 20% β), the texture is typically weaker and is similar to the rolling texture of single α alloys, with strong alignment of the basal 0002 poles along ND [6,11]. At higher temperatures and high β volume fractions (> 70% β) the room temperature α-texture is also weaker, mainly due to the randomising effect of phase transformation [6,8]. As it is challenging to measure, the β texture has not been studied as extensively as the α texture, but our recent work on Zr-2.5Nb [6] suggests that the strengthening of the α texture is accompanied by a strengthening of the β texture, when the volume fraction of α:β is about 50:50. With increasing β volume fraction, the α transverse texture component strengthens first, during which the β γ-fibre (111 in ND) disappears to be replaced by a very strong rotated cube component and a weaker $\{111\}\langle 112\rangle$ component [6].

Like the α texture, the β texture weakens at higher temperatures, and changes to the more common bcc α and γ fibre textures [6,10].

Since the β-phase is generally believed to be easier to deform than the α-phase at these temperatures [12], it is somewhat unexpected that strong characteristic textures develop in α + β alloys, dominated by single strong components in both phases. Deformation incompatibilities between the two phases would normally be expected to weaken the texture as the hard phase would be expected to cause the softer phase to deform around it [13], unless these incompatibilities are accommodated through a collaborative deformation process [14,15]. The fact that the textures in both phases then become much weaker at even higher temperatures, when there are fewer primary α and greater phase transformation on cooling, suggests that when the two phases are present in similar amounts ~ 50%, there is an "interaction" during deformation between the elongated primary α grains and surrounding β-matrix, which is responsible for the increased stability of the transverse α texture component, and strengthening of the β rotated cube component [6]. Nevertheless, so far, a convincing explanation for the origin of strong coupled single component texture in both phases has eluded the community. The absence of this physical understanding could also explain why models of texture evolution are still unable to quantitatively predict strengthening of the 0002||TD relative to the 0002||ND components during hot working [10,15–17] or the accompanying β texture [15].

The work presented here aimed to uncover the origins of both the coupled strengthening of characteristic α and β textures, and their weakening at high β volume fractions. A model Zircaloy-4 alloy with 7 wt.% Nb addition was hot-rolled and characterised using electron backscatter diffraction (EBSD). This alloy composition was chosen to lower the β transus temperature and inhibit phase transformation on air cooling [18,19], preserving the as-deformed microstructure for post-mortem examination using EBSD. The model alloy was hot-rolled at 725°C, corresponding to a β volume fraction of 70% (see *supplementary figures* for β approach curve). This phase fraction corresponds to a temperature of ~ 825°C in the Zr-2.5Nb alloy studied previously [6]. This rolling temperature is particularly interesting because it shows both strengthening of the α and β texture at moderate reductions and a slight weakening of the β-texture at higher reductions [6]. EBSD analysis was carried out using conventional 2D maps at two different spatial resolutions, supplemented by a 3D reconstructed volume of one of the samples. The results suggest that as well as co-deformation, recrystallization and phase transformation should be considered when explaining the coupled texture changes in the two phases seen during α + β processing.

2 Experimental procedures

2.1 Material and pre-processing

A model alloy, based on Zircaloy-4 with the addition of 7 wt.% Nb (subsequently referred to as a +7Nb alloy), was produced by induction skull melting, followed by gravity casting and air-cooling. The full chemical composition is given in Table 1. The cast $100 \times 40 \times 40$ mm block was first homogenised and rolled in the β-phase field to reduce the initial β-grain size and to develop a strong α-phase starting texture (with basal poles aligned in RD) for the subsequent rolling trial. This pre-processing consisted of β hot-rolling at 850°C with the ND/TD directions being alternated after each rolling pass, to form a work-piece measuring $350 \times 24 \times 16$ mm, followed by extended annealing at 750°C for 5 days and furnace cooling, to ensure chemical homogeneity in both phases.

Table 1: Chemical composition of the Zircaloy-4 + 7 wt.% Nb alloy.

	Zr	Nb	Sn	Fe	Cr
Zircaloy-4 + 7 wt.% Nb	91.80%	6.63%	1.23%	0.22%	0.12%

Note, results have been determined by energy dispersive X-ray fluorescence (EDXRF) analysis using the PANalytical MiniPal4 equipment and software package.

2.2 Rolling experiments

The +7Nb alloy was rolled at 725°C in two-stages to 50% ($\varepsilon_t = -0.7$) and 75% ($\varepsilon_t = -1.4$) reduction. A small $85 \times 17 \times 7.5$ mm block of the +7Nb starting material was first unidirectionally rolled to a 50% reduction, through 4 passes of 16%. A section of this material was then further rolled to 75% reduction with the same percentage reduction per pass. Rolling was conducted using lubricated 254 mm diameter rolls at a linear speed of 177.8 mm s^{-1}(35 ft min^{-1}), with a roll speed of 1.4 rad s^{-1} (13.37 rpm). The average effective strain rate therefore varied from about 2 s^{-1} in the first stage to about 4 s^{-1} in the second stage. The material was held at temperature (725ºC) for 1 hour prior to rolling, to ensure a homogeneous temperature distribution. To maintain the rolling temperature, heating was applied for 2 minutes between each pass, and the temperature recorded as the block was returned to the furnace by a thermocouple placed underneath the slab. Temperature drops of up to 100°C below the deformation temperature were measured at the surface after each rolling pass, and the temperature also dropped ~ 150°C during sample sectioning between the two rolling stages. Following sectioning, the block was returned to the furnace for up to 5 minutes to return to temperature before further rolling. On completing rolling, the blocks were air-cooled. Some samples were also subsequently annealed for 2 hours at 750°C in a tube furnace with Ar purge and cooled within the furnace at a rate of less than 1°C s^{-1}.

2.3 Characterisation

Samples were extracted from the centre of the rolled material for microstructural examination using optical microscopy and EBSD. They were ground to 4000 grit and polished using a 5:1 solution of colloidal silica and hydrogen peroxide. EBSD analysis was performed using a CamScan MX2000 field emission gun scanning electron microscope (FEG-SEM) operated at 20 kV, equipped with an AZtecHKL EBSD system, with subsequent analysis performed using the Oxford Instruments Channel 5 software. Measurements of macro-textures were made with a 5 μm step size over a total area of around 10 mm^2. A similar total area was analysed during measurement of the starting texture, although in this case a 1.5 μm step size was chosen, owing to the finer α-lath structure. More detailed orientation maps were also recorded using a step size of 0.1 μm to resolve the deformation microstructure. This 2D EBSD dataset is available from the Zenodo repository [20].

Serial section EBSD, followed by 3D reconstruction, was used to characterise the morphology of the deformed microstructure of the material rolled to 75% reduction. Data was collected using a dual beam Thermo Scientific Helios Xe^+ plasma focused ion-beam SEM (PFIB-SEM), with automated sample rotation. The volume that can be analysed by this technique is currently modest, owing to the slow acquisition time, and so only one sample was taken from the 75% rolling reduction material. A region of interest was first selected from the 2D EBSD map. The sample was then lifted out and analysed following the procedure described in the *supplementary materials*. Each slice was EBSD mapped over an area of 50 × 50 μm, on the RD-TD plane, with indexing at 0.15 μm step size. Slices 0.1 μm in thickness were then removed across the RD-TD plane. The final data set with a total analysis volume of 44 × 50 × 50 μm consisted of 441 individual slices, all within one β-grain, and took ~ 4 days to collect. This 3D EBSD dataset is available from the Zenodo repository [21].

The 3D EBSD orientation data and morphology of the segmented α and β phases were reconstructed using the DREAM.3D software [22], which was also used to calculate the feature reference misorientation (FRM) and kernel average misorientation (KAM) distributions within each texture domain of interest. To reconstruct the data, a customised pipeline was developed within DREAM.3D, which is described in the *supplementary materials*. Following reconstruction, the final 3D dataset file was visualised using ParaView [23,24]. Details of the analysis using ParaView are also given in the *supplementary materials.*

3 Results

3.1 α-phase texture

The texture of the starting materials was not random and both α and β phases were measured by EBSD. In Figure 1 a)i) it can be seen that the α-phase had a very strong 0002 basal pole alignment with RD, as well as a strong prismatic alignment of $\langle 10\bar{1}0\rangle$ with TD and $\langle 11\bar{2}0\rangle$ with ND. This strong α texture is consistent with phase transformation from the β-phase which is dominated by the $\{111\}\langle 110\rangle$ component, as seen in Figure 1 b)i), generated by the final β rolling pass carried out on the starting material. Crucially, the starting material contained very few orientations with $\langle 0002\rangle$ aligned with the transverse direction and therefore the starting α texture was very different from the expected texture after rolling.

The EBSD indexing rates achieved after rolling were ~ 25% for the α-phase and ~ 65% as β-phase, which is consistent with the expected 30/70 α/β volume fraction at 725°C in this alloy, assuming mis-indexing rates are similar for both phases. After a reduction of 50%, the starting texture was transformed into the typical hot rolling texture [6]. A strong $\{11\bar{2}0\}\langle 10\bar{1}0\rangle$ component developed in the α-phase. This dramatic change in the texture can be best appreciated in the ODFs shown in the *supplementary figures*, which shows the replacement of the $\phi_1 = 90°$, $\Phi = 90°$, $\phi_2 = 0°$ component by the $\phi_1 = 0°$, $\Phi = 90°$, $\phi_2 = 0°$.

Further reduction to 75% weakened the basal pole maxima in TD (Figure 1 a)iii) and strengthened the 0002 pole intensity around ND, with a tilt of ~ 20° towards RD. At the same time as the basal alignment in TD weakened, the prismatic alignment of $10\bar{1}0$ in RD strengthened, and sharpened the $\{11\bar{2}0\}\langle 10\bar{1}0\rangle$ texture component slightly, as can be seen in the ODF sections. As a result, the texture strengthened, even though the 0002 poles were less well aligned with TD and spread towards ND, forming a continuous fibre in the ODF from the $0002||$TD to the $0002||$ND, which was also seen to appear after hot-rolling of Zr-2.5Nb [6].

After annealing, the α EBSD indexing rate increased to 65%, whereas only 20% of the points were indexed as β. This decrease in the number the β points indexed in the annealed materials was caused by the nucleation of very fine secondary α within the β-matrix, which could not be indexed. Annealing of the rolled samples mostly strengthened the $\{11\bar{2}0\}\langle 10\bar{1}0\rangle$ α texture component after both 50% (Figure 1 a)iv)) and 75% reductions (Figure 1 a)v)). The 0002 pole figures after annealing at 75% reduction show that alignment of the basal poles remains slightly split either side of TD and with a slight rotation towards RD in the rolling plane.

3.2 β-phase texture

Measuring the β texture in the starting material was difficult because of the coarse starting β-grain structure. Even though a large area was analysed, it contained only ~ 20 deformed β-grains, as well as smaller broken up β regions. Nevertheless, although the measurements are not truly statistically representative, they are sufficient to allow discussion of the relative texture development of the two phases and for comparison with the textures measured in our previous study on Zr-2.5Nb [6]. The evolution of the β texture is shown in Figure 1 b) using ODF sections taken at $\phi_2 = 45°$. The starting material had a very strong β $\{111\}\langle 110\rangle$ texture component on the γ-fibre, which is located at the centre of the ODF at $\phi_2 = 45°$, together with much weaker $\{001\}\langle 110\rangle$ rotated cube and $\{001\}\langle 100\rangle$ cube components. The relative intensities are probably influenced by the poor grain statistics, but the grain orientations are consistent with those expected after β rolling. Despite the small numbers of grains studied, the overall trend in texture development was consistent with a weakening of the original γ-fibre component and a strengthening of the rotated cube component, as seen previously [6]. After 50% reduction, the strength of the main γ-fibre component reduced (Figure 1 b)ii)) but the texture did not change significantly in character. However, after 75% reduction, the $\{001\}\langle 110\rangle$ rotated cube component strengthened appreciably, and the β $\{111\}\langle 110\rangle$ weakened to form a weak γ-fibre. This final β texture is very similar to that produced following hot-rolling of Zr-2.5Nb at 825°C [6].

As expected, annealing at the rolling temperature did not measurably change the β-texture, which agrees with our previous work on a Zr 2.5Nb alloy [6]. The ODFs suggest that the annealed texture had a slightly stronger rotated cube component, but this difference could just be due to sampling variability caused by the large starting β-grain size.

3.3 Microstructure evolution

The starting microstructure of the +7Nb material after the β-pre-processing and annealing procedure is shown in Figure 2 a). The α-phase, which makes up ~ 50% of the alloy at room temperature, was present as single variant (colonies) of Widmanstätten laths within the β-grains. There were also a few allotriomorphic α-grains, which formed preferentially along the prior β grain boundaries, and along sub-grain boundaries within the β-grains.

After a 50% rolling reduction, the microstructure developed a range of different globular and elongated primary α grains (in Figure 2 b) and c)), which were predominantly aligned with the rolling direction. At 75% reduction, the volume fraction of elongated primary α grains increased,

and the number of low aspect ratio grains decreased, with many α-grains appearing to lengthen along RD. Annealing and slow furnace cooling caused the α volume fraction to increase to ~ 70%, but rather than nucleating new finer secondary α, the hcp phase mainly grew from the existing spherical and elongated primary α grains produced during rolling, as can be seen in Figure 2 d) and e). Only very fine secondary α-laths formed between the boundaries of the larger primary α in the annealed material at 75% reduction. These annealed microstructures resemble those seen following high temperature rolling and air-cooling of Zr alloys with lower Nb additions, like Zr-2.5Nb, except with a lower secondary α volume fraction appearing at room temperature [7,9,25]. The overall implication of these results is therefore that this alloy appears to deform similarly to other dual-phase Zr and Ti alloys and confirms it is a good model material with which to investigate the deformed state of the primary α and β-matrix.

3.4 Micro-texture development

The evolution of crystallographic orientations in the α and β phases during deformation are shown in the coarse scale EBSD maps in Figure 3 a) and b). The reference direction used in all inverse pole figure (IPF) maps is the TD direction, and therefore α-grains with 0002||TD are shown as red. At the start, the β-matrix was made up of grains elongated along RD with an aspect ratio of about 5:1 within which some misorientation was evident, introduced by the pre-processing. The α-grains present had many different starting orientations with very few grains initially orientated to be aligned with 0002||TD.

At 50% reduction, β-grain breakup was limited, although the grains were more elongated along RD and had an aspect ratio of ~ 10:1, consistent with the imposed reduction. After 75% reduction, however, grain breakup was very evident, with most grains developing into bands of different orientations aligned with the rolling direction. These bands of different β texture components in the starting and deformed materials have been separated out in Figure 3, showing the main {111}⟨110⟩ grains at 50% reduction, which were mostly present in the starting material, breaking up to form bands of the {111}⟨112⟩ and {001}⟨110⟩ orientations after 75% reduction. The appearance of these bands corresponds to the overall texture weakening and the strengthening of the rotated cube component observed.

This breakup of the β-grains occurred simultaneously with the evolution and then breakup of strong primary α micro-textures contained within them. The range of primary α variants present within different β-grains is plotted in the α 0002 pole figures in Figure 4. By 50% reduction the α texture

changed rapidly and there is evidence of extensive dissolution of different primary α variants in each of the β-grains. Compared to the starting material, four α variants were missing at the centre of the pole figure in the cube and rotated cube grains; whereas α-grains with 0002||RD, which was the strongest orientation in the starting material, had either been completely removed from the micro-texture or appeared with significantly reduced strength in the rotated cube, {111}⟨110⟩ and {111}⟨112⟩ grains. In all cases, the formation of the 0002||TD, or the ⟨0002⟩ aligned between RD-TD in the case of the cube grain, became the strongest orientation during deformation. These similar α orientations were distributed in bands that aligned with the rolling direction of the material, as seen in Figure 3 a). In most regions, this strong alignment of α in TD was correlated with a strong alignment of β in TD, as could be expected from the pole figures in Figure 4.

The breakup of the α 0002||TD component coincides with the breakup of the larger β-grains. At 75% reduction, the α micro-texture became similar within all β-grains, as shown in Figure 4 iii). Although the 0002||TD remained the strongest component, there was a noticeable weakening of the basal pole alignment, along with the development of a greater spread of orientations aligned towards the centre of the pole figure, with 0002||ND. In the cube grains, the α component with ⟨0002⟩ aligned between RD-TD appeared to have been so unstable that it rapidly disappeared from the micro-texture with strain, leaving behind a spread of orientations, at the centre of the pole figure, which corresponded with the breakup of these highly elongated β-grains seen in Figure 3 c)iii).

Comparing the orientation maps before and after rolling, in Figure 5, Figure 6 and Figure 7, shows very clearly the dramatic change in α texture. Originally distributed in packets tens of microns in size, rolling to 50% produces much larger micro-texture regions of similar α-grain orientations, containing only a single primary α orientation in some cases, as shown in Figure 6. At just 50% reduction, region 1 in the top half of the orientation map shown in Figure 6, which corresponds to a single β-grain with a main {111}⟨110⟩ γ-fibre component, can be seen to contain only α with only a single 0002||TD orientation. In region 2, in the bottom half of the map in Figure 6 with a β {001}⟨100⟩ cube orientation, most of the α-grains have their 0002 pole lying within the rolling plane, aligned at a greater angle of 45°, from TD to RD, with only a few grains with 0002||ND. However, in both regions, comparison of the α 0002 and β 110 pole figures showed that the orientations of the two phases retained their mutual Burgers orientation relationship, although there were high misorientation gradients across each of the grains.

The α-grain morphology and level of grain breakup clearly depend on crystallographic orientation. For example, α-grains with 0002||TD in region 1 and 0002||ND in region 2 are highly elongated in Figure 6, compared to grains with their basal pole aligned in the rolling plane in region 2. These elongated thin ribbon grains with 0002||TD did not break up, although there was a large orientation spread in the $11\bar{2}0$ pole figure, with rotation axis in TD, most likely caused by prismatic slip. On the other hand, the α elongated grains with 0002||ND did break up, showing very high misorientation gradients along their length and the formation of new internal high angle grain boundaries. The spread of orientations in the local β-matrix was also different in the two regions, as can be seen in the pole figures in Figure 6, which suggests it was affected by the stability of the main primary α grain orientations.

The breakup of the β-grains into micro-texture bands seems to depend on the primary α orientations, as can be seen after 75% reduction in Figure 7. In the top (region 1) and bottom (region 3) bands of the map, both β-grains lie close to the {111}⟨110⟩ component of the γ-fibre, but contain very different orientations of α. Band 1 contains mostly small and broken up "globular" α, which have ⟨$11\bar{2}0$⟩ parallel to TD and a spread of 0002 basal poles clustered around ND, with some spread toward RD. These α orientations, which were predominant in the starting material, coincide with very high local misorientations in the surrounding β-matrix, seen as a spread in the β pole figure. In contrast, in region 3, at the bottom of the map, the α-grains are highly elongated in the rolling direction, with 0002||TD and this sharp transverse texture component, and high elongation, coincides with a much lower misorientation within the surrounding β-matrix.

The more pronounced breakup of the cube grain in region 2, at the centre of the map in Figure 7, includes α morphologies with a wide range of both globular and lamellae grains that had a distribution of basal poles aligning between ND and TD. Many of these stringers of broken up α-grains have different orientations, producing a spread around ND in the micro-texture, in Figure 4 a)iii). These broken up stringers of different α orientations coincide with a much greater breakup of the local β-matrix, which have developed new sub-grains with primarily rotated cube orientation.

3.5 Three-dimensional EBSD analysis

Two-dimensional EBSD maps are limited in their ability to reveal the real 3D shape of the α-grains dispersed within the β-matrix, or their connectivity. To overcome this limitation, serial sectioning was carried out using a plasma FIB, to produce a sequence of slices from the material rolled to 75% reduction that could be reconstructed into a 3D volume. Continuous misorientation boundaries

greater than 5° were used to segment individual α-grains. Although 5° is a somewhat arbitrary distinction, it was chosen to best isolate different α-grains, whilst still capturing sub-grain boundary features with misorientations of less than 5°.

The full reconstructed volume is shown in Figure 8, along with the average micro-texture obtained from the 3D data set for each phase. In the volume analysed, the β-phase is revealed as a continuous matrix within which individual α-grains are seen to be preferentially elongated along RD and extending beyond the volume analysed. This volume was studied in an attempt to capture a small representative micro-texture band, like the ones seen in the 2D maps, which contains α-grains of different orientations within a misoriented β region. The orientation of the β-grain matrix studied was near $\{111\}\langle 110\rangle$, which is a component from the γ-fibre that weakens with increasing reduction. In Figure 8 b) it can be seen that there was a measurable spread of the β orientations, which was mostly made up of a rotation around {111} and ND. The accompanying α-phase pole figures in Figure 8 a) show one main component: $\langle 0002\rangle$ tilted slightly off-axis by 10° away from TD, and alignment of $\langle 11\bar{2}0\rangle$ with ND. Other α-grains have different orientations, some with $\langle 0002\rangle$ tilted off-axis 10° in the opposite sense from TD and a few with basal poles aligned with ND.

The shape of the grains depends strongly on their orientation. The overwhelming majority of α-grains have an 0002 pole aligned with TD and are shaped like flat elongated ribbons, very thin along ND and elongated along RD, as shown at the top of the 3D volume (region 1) in Figure 8 and in each of the three grain morphologies in Figure 9 c). These α-grains correspond to the elongated grains seen in the 2D EBSD maps and were found throughout the extracted cube, dominating at the top and bottom in particular. The highly elongated α-grains were approximately 1 μm thick and 5 μm wide. Most of these elongated grains were longer than 50 μm, although it was not possible to determine their length with certainty as they do not start or end in the sampled volume. The long axis of these grains was slightly misaligned along RD by 10°, which coincides with the slight off-axis tilt of the $\langle 0002\rangle$ 10° from TD seen in the α-phase pole figures. This suggests the shape of these grains is determined by their crystallography and not the plane strain deformation of the sample, with flattening of the grains seen along $\langle 11\bar{2}0\rangle$ and elongation along $\langle 10\bar{1}0\rangle$.

Just below the top region of the data set (region 2 in Figure 8), a number of differently orientated primary α grains also existed that had their basal poles orientated parallel with ND. These grains had different, wider in TD, more bent, plate-like morphologies, as seen in Figure 9 a). The edges of

these grains had high curvatures, particularly at highly misorientated regions, which is compelling evidence for grain boundary migration through ingress of the β-phase.

3.5.1 Dependence of misorientation and stored energy on grain orientation

In the 3D dataset, the misorientation within the α-grains varied systematically with their orientation. The flat, elongated grains belonging to the dominant $\{11\bar{2}0\}\langle 10\bar{1}0\rangle$ component, that have been separated out in Figure 9 c), tend to show low misorientation gradients within the grain and a low misorientation spread in the pole figure, which suggests this crystallographic component is stable, whereas grains with $\langle 0002\rangle$ aligned close to ND contained higher misorientations throughout the grains and developed larger crystal rotations, with a spread around $\langle 0002\rangle$ and ND of over $45°$. These higher internal misorientations were accommodated in sub-grain boundaries, which are clearly shown by the KAM measurements performed across the different grains that are presented in Figure 9 a). The distributions of KAM values were calculated with a kernel size of $3 \times 3 \times 3$ cells (equivalent to a voxel of $2.25\ \mu m^3$) and are given in Figure 8. This revealed that the "stable" grains that strengthen the texture during rolling, with a transverse basal texture component, tended to contain sub-grains with lower KAM angles than other α orientations – with median values for these grain types of $0.45° \pm 0.03°$ compared to $0.73° \pm 0.01°$ for the $0002||ND$ aligned grains.

KAM distribution measurements also revealed differences in the local sub-structure within the surrounding β-matrix, that related to the crystallographic orientation of the embedded primary α grains it surrounded. In this case, the analysis was conducted by selecting two different regions in the β-grain. In region 1, the β-grain contained mostly α with a transverse texture component, whilst region 2 predominantly contained α-grains of other different (mainly $0002||ND$) crystallographic orientations. According to Figure 8 b), a lower average β-matrix KAM distribution was found in region 1 (with a median of 0.4°), compared to region 2 (with a median of 0.5°). Surrounding these $0002||ND$ grains, the β-grain was found to be more highly misorientated and also contained a higher density of sub-grains. Overall, these results are therefore consistent with the matrix β bands containing α-grains aligned with $0002||ND$, which are typically "harder" orientations in the single-phase case, having larger local misorientations.

The KAM data was further used to estimate the relative stored energy within specific α orientations, following the method proposed by Godfrey, Mishin and Yu [26], which has been shown to give reliable estimates. A step size of less than 1/5 of the average sub-grain size is required to accurately estimate the stored energy of deformation, which was met in our analysis, as well as the choice of a

cut-off angle chosen during averaging [26]. Here, the high cut off was set at 5°, since few boundaries within individual texture domains were found to exceed 3° (Figure 8) and misorientations greater than this were classified as boundaries to segment the 3D EBSD data between different texture components.

According to Godfrey et al. [26] the local stored energy, E_s, at each voxel can be estimated based on the θ_{KAM}, of a voxel compared to its 6 nearest-neighbour voxels, using the equation;

$$E_s = \frac{3Gb}{2\Delta}\theta_{KAM}$$

Equation 1

where G is the shear modulus, b is the Burgers vector and Δ is the step size. Performing this calculation using an average KAM value, determined from the voxels within a grain volume, was used to provide an estimate of the volume averaged stored energy within a given α micro-texture domain. The relative differences between the stored energy calculated by this method are equivalent to the relative differences in volume averaged misorientation, since the multiplying factor ($3Gb/2\Delta$) is a constant. The shear modulus and the Burgers vector for prismatic slip were assumed to be 23.6 GPa [27] and 0.32 nm [28], respectively. Using this approach, the stored energy contained within the "harder" α basal $0002||\mathrm{ND}$ components was determined to be around $160 \pm 20\ \mathrm{MJ/m^3}$, which was over 1.6 times more than the value of $98 \pm 7\ \mathrm{MJ/m^3}$ estimated for the "softer" $0002||\mathrm{TD}$ orientated primary α grains. Similarly, the stored energy was found to be 1.3 times higher in the β-matrix regions surrounding the "harder" α orientations at $123\ \mathrm{MJ/m^3}$, compared with $95\ \mathrm{MJ/m^3}$ in the matrix surrounding α with the "soft" transverse texture component.

4 Discussion

4.1 Texture development

The macro-texture results confirm that the texture development in the model +7Nb alloy is consistent with that observed in other dual-phase Zr and Ti alloys rolled to the same strains, at equivalent phase fractions. Despite their different starting textures, the α texture evolution in the model alloy is remarkably similar to that in Zr-2.5Nb [6] and Ti-64 [8,9] when processed at an equivalent β volume fraction of 70%. Since only primary α was retained on cooling in the model alloy, the similarity in the α-textures after rolling confirms that the strong transverse basal texture is

characteristic of the deformed primary α and is not generated from transformation of the deformed β on cooling by strong variant selection [29–33].

The primary α texture develops rapidly with strain, and the main $\{11\bar{2}0\}\langle 10\bar{1}0\rangle$ component is established after only 50% reduction, strengthening through alignment of $\langle 10\bar{1}0\rangle$ along RD after 75% reduction, even though the 0002 pole intensity weakens slightly. This rapid α texture change occurs within β-grains that change their orientation much more slowly, and that noticeably fail to break up until the larger 75% reduction. The β texture also changes with rolling, but much more gradually, through the characteristic strengthening of the dominant rotated cube component that has previously been seen in both Zr and Ti alloys processed at equivalent temperatures [6,10] and the weakening of the initially present {111}<110> component which spreads into a weak γ fibre, and by developing a small amount of Goss component [7].

4.2 Mechanisms of texture development

Although the development of a strong $\{11\bar{2}0\}\langle 10\bar{1}0\rangle$ primary α texture in the model alloy confirms that this texture component forms during deformation, there is evidence that this texture change did not happen through plasticity alone. There has been only limited crystal plasticity modelling of the texture evolution during hot deformation of α + β alloys [15,16], both using viscoplastic self-consistent (VPSC) modelling, from which it is difficult to infer how quickly this transverse texture component develops and how fast the grains with $\langle 0002\rangle$ aligned along RD disappear. In the work by Lebensohn and Canova, results are only shown for a reduction of 70% (ε = 1.2) at a low β volume fraction (20%) [15]. Although their results show a general weakening of the 0002 poles along RD after a large deformation, the starting texture is random, unlike here where the starting 0002||RD pole was very strong. In the forging texture simulations by Glavicic et al., the 0002||RD also seems to consistently survive significant reductions [16], whereas experimentally it disappears. Crystal plasticity modelling of hot single-phase α deformation confirms that it is difficult to explain the disappearance of this component though slip in α alone. In Logé et al., VPSC always predicts strong 0002||RD alignment after plane strain deformation [34] and in Prakash et al., strong components with 0002||RD only weaken slightly with deformation [35]. The simulations by Lebensohn and Canova do show that the development of the 0002||TD alignment itself can be partly predicted by VPSC modelling after large reductions, by coupling the deformation of the two phases using realistic grain shapes [15]. Even then, the predicted $\langle 0002\rangle$ alignment is relatively weak, which is unusual for a VPSC model, as it tends to over-predict texture strengths [36].

There are other more direct indications that the α texture change is not solely due to plasticity. It appears very rapidly with strain, and there is no evidence of a fibre linking the starting α orientations to those of the stable end texture components, which would be expected for a gradual texture change involving crystal rotation driven by plastic slip. Rather, it is as if the α-grains with ⟨0002⟩ along RD and ND quickly disappear and are replaced, at least in part, by grains with ⟨0002⟩ along or near TD. During cold working, such fast texture changes have been attributed to twinning [37,38], but not only is twinning unlikely at these high temperatures [39,40], it also cannot explain the changes in orientation that are observed. The only twinning mode capable of such a dramatic orientation change is the $\{10\bar{1}2\}\langle\bar{1}011\rangle$ tension twin, which reorients the ⟨0002⟩ towards ND and not towards TD, as is observed in [35]. In a separate study on Zircaloy-4 [34], the 0002||TD poles are stronger after plane strain deformation at higher temperatures (750°C), when the starting microstructure is finer. In the same article, it was proposed that this texture change is driven in part by "metadynamic" recrystallization, without which the disappearance of the 0002||RD aligned α cannot be explained. However, it is more difficult to see how recrystallization on its own could explain the disappearance in our rolling experiments, where the α volume fraction is only 30% and non-contiguous.

Another possible explanation for this dramatic texture change is variant selection via phase transformation, occurring either dynamically during rolling, or statically between each reduction step. Dynamic phase transformation is known to happen during hot deformation of steels [41] and has recently also been reported in Ti-64 [42–44]. Phase transformation can also be driven by temperature transients during rolling: the temperature will decrease and α re-grow as the sample is removed from the furnace and temperature increases again during deformation and during reheating, where the β would be expected to expand, or it could be driven by stress during rolling [3,31,45,46]. This alloy has a high Nb content, which has very low solubility in α [18,19]. Nb is also a slow-diffusing, β stabilising species [19], and therefore phase transformation in this alloy is very slow, which is why secondary α was suppressed on cooling. A slow, diffusion-controlled phase transformation will limit the amount of static phase transformation that can occur during the transient temperature changes experienced during the rolling schedule. However, since the diffusivity of Nb increases with dislocation density, deformation could potentially promote transformation by enhancing Nb transport, and increase the driving force by affecting the stored energy in each phase.

The most compelling indication of the involvement of phase transformation is the way the α texture changes for different parent β orientations. As Figure 4 shows, α variants with ⟨0002⟩ along RD

and ND essentially “disappear” after 50% reduction and there is a strengthening of the 0002 poles near TD within all main β grain orientations. However, the details of this 0002||TD strengthening are different for different β orientations. For the β rotated cube and the {111}⟨112⟩ component of the γ fibre, there is very good alignment of α ⟨0002⟩ with TD. However, for the β cube and {111}⟨110⟩ orientations, the α 0002 poles are not as well aligned with TD. Instead, they seem to lie in between the initial position, with ⟨110⟩ in the β, and the TD direction. The 3D EBSD sectioning shows that this misalignment is possible because of the morphological misalignment of the elongated primary α grains with the rolling direction. Like the long, thin α-grains which are crystalographically well aligned with TD in the β rotated cube grains, these grains are elongated along $\langle 10\bar{1}0\rangle$, but misaligned with TD, suggesting they start off with ⟨0002⟩ well aligned with ⟨110⟩ in the parent β grain and gradually become aligned towards TD as deformation proceeds, presumably through rotation due to plastic slip.

The 3D EBSD analysis provides some indication of how variant selection might occur, driven by a interface migration. As Figure 9 shows, the different α variants interact differently with the parent β-phase. Grains with ⟨0002⟩ near TD are elongated along $\langle 10\bar{1}0\rangle$ and have very low stored energy, whereas grains with other orientations have higher stored energy and are evidently being preferentially consumed by β, as shown in Figure 9 a). The orientation of the elongated 0002||TD grains is consistent with deformation via prismatic slip occurring on two symmetric slip systems that prevent crystal rotation and give rise to a high stability for this component [47]. Elongated grains with this stable orientation are commonly seen in cold worked Zr and Ti alloys, where they also show very little misorientation and low stored energy [48]. Their elongated thin, ribbon-like, morphology and the lack of misorientation in the surrounding β-phase surrounding them suggests that $\{11\bar{2}0\}\langle 10\bar{1}0\rangle$ α orientations are “soft”, and as easy to deform as the β. The other “hard” α orientations cause noticeable misorientation to develop in the surrounding β-matrix, giving rise to large misorientations and the development of a local β substructure in the form of sub-grains. These hard-oriented α-grains are also more unstable and develop large misorientations within them, made up primarily of rotations around the ⟨*c*⟩-axis, consistent with variations in prismatic slip rate. This difference in the local dislocation density, and stored energy, could explain the preferential selection of specific micro-texture volumes during deformation and thermal cycling, by enhancing Nb diffusion around and inside the unfavourable oriented α-grains, and encouraging their breakup and dissolution [49]. Although there was no obvious change in the overall phase fractions with rolling strain, small differences were difficult to confirm because EBSD indexing is only 90% successful. The EBSD maps do show apparent local differences in α volume fraction, with regions containing

elongated α showing higher local α volume fractions that increased by around 4% and 10%, as seen in Figure 6 and Figure 7, although this is difficult to confirm given the 2D nature of the data. The lack of a noticeable change in phase fraction, together with the development of large regions containing only elongated α, suggest that this dissolution of "hard" α orientations must be accompanied by growth or precipitation of the soft orientations, producing the observed fast texture change.

The changes in morphology confirm that all the primary α grains are deformable, although their rate of shape change depends on their strength relative to the surrounding β-matrix, which depends on their orientation. The lack of misorientations developing in the β surrounding the thin $\{11\bar{2}0\}\langle 10\bar{1}0\rangle$ aligned grains, seen in the 2D maps in Figure 6 and Figure 7 and the 3D analysis in Figure 8, implies that there is essentially no plastic incompatibility between them and the matrix. In other words, α-laths with a transverse orientation are not stronger than the surrounding β-phase. There is no evidence of rigid body rotation of "hard" α within a soft β-matrix [45,50], to align the $\langle 0002\rangle$ with TD. This local orientation dependence of how easily the two phases co-deform also implies that the macroscopic flow stress of material will decrease with the fast change in texture, contributing to the softening behaviour often seen during α + β hot deformation [36].

The EBSD maps show how the β texture development is also affected by interaction between the two phases, despite the relatively large starting β grain size making it difficult to interpret quantitative comparisons of the texture change. Since the material had been rolled in the β domain before this experiment, the starting β texture was relatively stable, which helps to explain the relatively low level of change after 50% reduction. Nevertheless, there is evidence, even at this stage, that the co-deformation of the two phases can promote the development of the rotated cube component and the disappearance of the $\{111\}\langle 110\rangle$ component. In the EBSD maps in Figure 7, small grains with rotated cube orientation can already be seen emerging inside the larger β-grains, between parallel α-laths. These new grains, made possible by a rotation about RD for the $\{111\}\langle 110\rangle$ grain and about ND for the cube-oriented grain, both align the $\langle 110\rangle$ direction with TD.

Although the rotated cube orientation is normally only a minor texture component in single-phase rolled bcc metals [51], it becomes more important as the deformation temperature increases and as the amount of reduction increases [52,53]. Crystal plasticity modelling of single β-phase deformation suggests that this component is favoured by high aspect ratio elongated, pancake grain shapes: when using the Taylor model, the component is favoured by relaxed constraints [29,54] and

when using the VPSC model, the rotated cube component is enhanced when elongated grains are used [52]. Modelling its development during dual-phase α + β deformation, however, seems to be less successful [10,15,16]. There is also evidence that, during hot deformation in the β-phase region, the rotated cube component is further enhanced by recrystallization, although it is not clear if this occurs during deformation, "metadynamically" at the end of deformation, or by both, which seems to depend on strain rate [55].

If the development of the rotated cube component is enhanced by large reductions and plane strain constraint, then it is plausible that the rotated cube is favoured by the constraint imposed by the embedded α-grains, especially if they are elongated along RD and deforming at the same rate as the β-phase, like the elongated α-grains seen here. Once a nucleus of rotated cube orientation develops, it can then also grow by interface migration: the misorientation within these new rotated cube grains does seem to be lower than the other β orientations around them. This mechanism can also help to explain why the γ fibre spreads away from the $\{111\}\langle 110\rangle$ towards the $\{111\}\langle 112\rangle$, as seen in the EBSD volume, since the latter can maintain alignment of one $\langle 110\rangle$ direction with the $\langle 0002\rangle$ along TD.

At greater reductions, the elongated 0002||TD α-grains become longer and thinner, and start breaking up through activation of pyramidal slip, perhaps as a result of the loss of constraint associated with the extreme grain shape, causing a weakening of the 0002 poles along TD and a spread around ND. Despite this, the $\{11\bar{2}0\}\langle 10\bar{1}0\rangle$ texture component strengthens, as prismatic slip continues to strengthen the $\langle 10\bar{1}0\rangle$ alignment with RD. In the β-phase, the local conditions that lead to the spreading out of the $\{111\}\langle 110\rangle$ component along the γ-fibre become more widely established, leading to a strengthening of the $\{111\}\langle 112\rangle$ component and of the rotated cube component, eventually leading to β grain breakup in the form of parallel bands of alternating texture components.

Annealing leads to a slight enhancement of the α components formed following high temperature deformation, primarily because the primary α grows during annealing and subsequent slow cooling, as can be seen in Figure 2. The precipitation of secondary α does produce a measurable increase in the $\langle 0002\rangle$ along RD during heat treatment, but overall the texture is essentially unchanged.

4.3 Texture evolution with α/β volume fraction

Although only one rolling temperature was studied, the mechanisms of texture evolution discussed above can be used to explain the texture evolution seen more generally during hot-working of α + β alloys at different temperatures and different phase fractions. Although the $0002||TD$ component typically only develops at higher temperatures in the dual-phase case, it can also develop at low β volume fractions [6] and even in a single-phase α alloy [34]. Since it cannot be easily explained by plasticity alone, it must be driven by diffusion-controlled interface movement, either within the α-phase, by recrystallization, or by deformation assisted phase transformation. This mechanism requires differently oriented α-laths to either be in contact or in close vicinity. Therefore, it will be more difficult in coarse colony microstructures produced by slow cooling, than in basket-weave microstructures produced by faster cooling, which is consistent with previous experimental observations of globularisation in Ti alloys [56].

It is the development of the $\{11\bar{2}0\}\langle10\bar{1}0\rangle$ α component, in the form of highly elongated stable α-grains, that sets up the conditions necessary for the strengthening of the rotated cube component. Previous work on Zr-2.5Nb showed that strengthening of the rotated cube component peaks at a temperatures where the β volume fraction is 50%, whereas the α texture strength peaks at a slightly lower temperature [6]. However, these previous α texture measurements included both primary and secondary α. Since secondary α is produced by transformation on cooling, post deformation, it will probably weaken the measured texture, which implies the primary α texture was in all likelihood stronger at the original processing temperature, consistent with the idea that the $\{11\bar{2}0\}\langle10\bar{1}0\rangle$ α and $\{100\}\langle110\rangle$ β components develop synergistically. A higher α volume fraction implies thicker, elongated $\{11\bar{2}0\}\langle10\bar{1}0\rangle$ α-grains that can remain stable to larger reductions than the same grains at higher temperature, establishing the conditions to form the strong, coupled α and β textures found at these temperatures. The $\{11\bar{2}0\}\langle10\bar{1}0\rangle$ α stabilises the $\{100\}\langle110\rangle$ β orientation and vice versa, because they can deform in a compatible manner, with low interphase stresses and generating low stored energies in both phases.

This reasoning can also be used to explain the texture weakening as the temperature increases towards the β transus. At higher temperatures and higher β volume fractions, the α volume fraction is too small to provide the morphological constraints required to stabilise the rotated cube component [6,10]. Instead, the primary α grains act more like hard particles in a soft β-matrix, causing the β texture to weaken around the typical bcc α and γ fibres [6,10]. The α texture after deformation at high temperatures and high β volume fractions is dominated by transformed α nucleating in weakly textured β, and is therefore usually very weak. Above the β transus, the

randomising effect of α is no longer present and therefore the β textures strengthen, as does the α texture produced by transformation on cooling [6], especially if variant selection occurs [9,57].

4.4 Implications for processing and modelling of dual-phase processing

Some aspects of the texture development described can be successfully predicted by self-consistent plasticity modelling, but only when interactions between the two phases are explicitly imposed [15]. However, the textures predicted are too weak, and only develop after large imposed deformations, whereas in practice the ⟨0002⟩ alignment with TD appears very rapidly, and is accompanied by the disappearance of α-grains with ⟨0002⟩ along RD and ND. This rapid development of the $\{11\bar{2}0\}\langle 10\bar{1}0\rangle$ component must therefore require recrystallization and/or phase transformation, and thus cannot be predicted by crystal plasticity modelling alone. Since the development of the rotated cube component requires the presence of a strong α texture, it is unsurprising that the same models fail to predict the development of the rotated cube β texture component [10,15,16], although it is possible that the β volume fraction simulated was too low. Given the strong correlation required for the development of this component, the VPSC formulation might need to be further modified to explicitly include more details of the α-β interaction.

Further development of mean field models should probably be accompanied by full-field modelling of small volumes, using frameworks like phase field modelling that can account for chemistry effects and that allow grain and phase boundary movement [58,59]. Such models would better enable the parameterisation of the morphological changes and provide a better understanding of the contributions of diffusion-controlled orientation selection and kinetics of phase transformation, and how this interacts with texture evolution caused by slip. Such full-field models will be complex and will require the identification of many different parameters and their development will rely on the availability of phase fraction and texture data obtained *in-situ* at representative strain rates and temperatures, that can only be obtained with fast synchrotron X-ray diffraction experiments [60].

One technological implication of this work is that the rapid texture changes seen after small reductions produce contiguous regions of similarly aligned primary α, which are often called *macrozones* in the Ti-64 literature [61–65]. Macrozones have historically been thought to originate from a lack of microstructure breakdown, but the results here show that they can develop during hot deformation by strong texture reinforcement, even when they are not present at the start. Another implication is that the rate of texture change will be affected by the starting microstructure and texture. For example, orientation selection through recrystallization requires differently oriented α

variants to be close together and therefore will happen more rapidly in regions where the cooling rate is faster and colonies are smaller. Although the effect of colony orientation on α breakup has been studied before [66,67], this work suggests that the size of the α-grains and the distance between different variants is an important parameter that has been overlooked. Also important is the starting β texture, since it influences how quickly the α texture develops, which in turn affects how quickly the rotated cube component develops [6].

5 Conclusions

By studying the texture development in a model Zr-Nb alloy, we have shown that the texture evolution during hot working depends on the interaction between the two phases and involves recrystallization and phase transformation, as well as plastic deformation. The texture changes in α precede those of β and seem to be the result of contributions of diffusion-controlled orientation selection through recrystallization and phase transformation, with the harder to deform primary α grains essentially dissolving into the β-matrix to be replaced by easily deformed elongated α-grains with low stored energy. The majority of these elongated α-grains have a $\{11\bar{2}0\}\langle 10\bar{1}0\rangle$ orientation, which promote the development of the rotated cube orientation in the β-phase, the strong texture components typically found in hot-rolled, dual-phase Ti and Zr alloys that are difficult to predict through crystal plasticity modelling alone. These findings have implications for process control and modelling of the texture evolution during processing of these important alloys.

6 Acknowledgements

This research is sponsored by Rolls-Royce plc. and the UK's Engineering and Physical Sciences Research Council (EPSRC) via the Nuclear Engineering Doctorate (EngD) programme and LightForm (EP/R001715/1).

7 Data statement

All data presented here is available from the LightForm community in the Zenodo repository [20,21].

References

[1] S. Banerjee, Nuclear Applications: Zirconium Alloys, in: K.H. Cahn, R.W. Flemings, B. Ilschner, E.J. Kramer, S. Mahajan, P. Veyssière (Eds.), Encycl. Mater. Sci. Technol., Elsevier Science Ltd., 2001: pp. 6287–6299. doi:10.1016/B0-08-043152-6/01117-7.

[2] G. Lütjering, Influence of processing on microstructure and mechanical properties of (α+β) titanium alloys, Mater. Sci. Eng. A. 243 (1998) 32–45. doi:10.1016/S0921-5093(97)00778-8.

[3] R.A. Holt, S.A. Aldridge, Effect of extrusion variables on crystallographic texture of Zr-2.5 wt% Nb, J. Nucl. Mater. 135 (1985) 246–259. doi:10.1016/0022-3115(85)90084-4.

[4] Y. Li, R. Rogge, R.A. Holt, Development of local microstructure and crystallographic texture in extruded Zr–2.5Nb tubes, Mater. Sci. Eng. A. 437 (2006) 10–20. doi:10.1016/j.msea.2006.04.048.

[5] N. Saibaba, K. Vaibhaw, S. Neogy, K. V. Mani Krishna, S.K. Jha, C. Phani Babu, S. V. Ramana Rao, D. Srivastava, G.K. Dey, Study of microstructure, texture and mechanical properties of Zr-2.5Nb alloy pressure tubes fabricated with different processing routes, J. Nucl. Mater. 440 (2013) 319–331. doi:10.1016/j.jnucmat.2013.03.069.

[6] C.S. Daniel, P.D. Honniball, L. Bradley, M. Preuss, J. Quinta da Fonseca, A detailed study of texture changes during alpha–beta processing of a zirconium alloy, J. Alloys Compd. 804 (2019) 65–83. doi:10.1016/j.jallcom.2019.06.338.

[7] C.S. Daniel, P.D. Honniball, L. Bradley, M. Preuss, J. Quinta da Fonseca, Texture Development during Rolling of α + β Dual-Phase ZrNb Alloys, in: Zircon. Nucl. Ind. 18th Int. Symp., ASTM International, 100 Barr Harbor Drive, PO Box C700, West Conshohocken, PA 19428-2959, 2018: pp. 151–179. doi:10.1520/STP159720160070.

[8] M. Peters, A. Gysler, G. Lütjering, Control of microstructure and texture in Ti-6Al-4V, in: H. Kimura, O. Izumi (Eds.), Titan. '80, Sci. Technol. Proc. Fourth Int. Conf. Titan., Metallurgical Society of AIME, Kyoto, Japan, 1980: pp. 1925–1935.

[9] H. Inagaki, Evolution of textures and microstructures in thermomechanical processing of Ti-6Al-4V, Zeitschrift Für Met. 81 (1990) 433–445.

[10] D. Dunst, H. Mecking, Analysis of experimental and theoretical rolling textures of two-phase titanium alloys, Zeitschrift Für Met. 87 (1996) 498–507. http://cat.inist.fr/?aModele=afficheN&cpsidt=3142129 (accessed July 9, 2015).

[11] E. Tenckhoff, Review of Deformation Mechanisms, Texture, and Mechanical Anisotropy in Zirconium and Zirconium Base Alloys, J. ASTM Int. 2 (2005) 25–39.

[12] S.L. Semiatin, T.R. Bieler, The effect of alpha platelet thickness on plastic flow during hot working of TI–6Al–4V with a transformed microstructure, Acta Mater. 49 (2001) 3565–3573. doi:10.1016/S1359-6454(01)00236-1.

[13] F.J. Humphreys, M. Hatherly, The Deformed State, in: Recryst. Relat. Annealing Phenom., Elsevier, 2004: pp. 11–65. doi:10.1016/B978-008044164-1/50006-2.

[14] S. Suri, G.B. Viswanathan, T. Neeraj, D.-H. Hou, M.J. Mills, Room temperature deformation and mechanisms of slip transmission in oriented single-colony crystals of an α/β titanium

alloy, Acta Mater. 47 (1999) 1019–1034. doi:10.1016/S1359-6454(98)00364-4.

[15] R.A. Lebensohn, G.R. Canova, A self-consistent approach for modelling texture development of two-phase polycrystals: Application to titanium alloys, Acta Mater. 45 (1997) 3687–3694. doi:10.1016/S1359-6454(97)00067-0.

[16] M.G. Glavicic, R.L. Goetz, D.R. Barker, G. Shen, D. Furrer, A. Woodfield, S.L. Semiatin, Modeling of Texture Evolution during Hot Forging of Alpha/Beta Titanium Alloys, Metall. Mater. Trans. A. 39 (2008) 887–896. doi:10.1007/s11661-007-9376-2.

[17] S.L. Semiatin, S.V. Shevchenko, O.M. Ivasishin, M.G. Glavicic, Y.B. Chun, S.K. Hwang, Modeling and simulation of texture evolution during the thermomechanical processing of titanium alloys, in: ASM Handb. Vol. 22A Fundam. Model. Met. Process., Tenth Edit, Materials Park, OH, 2009: p. 536.

[18] S. Banerjee, Displacive and Diffusional Transformations of the Beta Phase in Zirconium Alloys, in: Zircon. Nucl. Ind. 17th Vol., ASTM International, 100 Barr Harbor Drive, PO Box C700, West Conshohocken, PA 19428-2959, 2015: pp. 23–51. doi:10.1520/STP154320130039.

[19] M. Ivermark, J. Robson, M. Preuss, Measurement and Modeling of Second Phase Precipitation Kinetics in Zirconium Niobium Alloys, J. ASTM Int. 7 (2010) 150–175. doi:10.1520/JAI103011.

[20] C.S. Daniel, J. Quinta da Fonseca, 2D EBSD Dataset of the Alpha and Beta Phase Orientations for a Hot-Rolled Model Zircaloy-4 with 7 wt.% Nb Alloy, Zenodo. (2020). doi:10.5281/zenodo.3784461.

[21] C.S. Daniel, A. Garner, J. Quinta da Fonseca, 3D EBSD Dataset of the Alpha and Beta Phase Orientations for a Hot-Rolled Model Zircaloy-4 with 7 wt.% Nb Alloy, Zenodo. (2020). doi:10.5281/zenodo.3785085.

[22] M.A. Groeber, M.A. Jackson, DREAM.3D: A Digital Representation Environment for the Analysis of Microstructure in 3D, Integr. Mater. Manuf. Innov. 3 (2014) 5. doi:10.1186/2193-9772-3-5.

[23] J. Ahrens, B. Geveci, C. Law, ParaView: An End-User Tool for Large-Data Visualization, in: Vis. Handb., Elsevier, 2005. doi:10.1016/B978-012387582-2/50038-1.

[24] U. Ayachit, The Paraview Guide: A Parrallel Visualization Application, Kitware, 2015.

[25] C.S. Daniel, An Investigation into the Texture Development during Hot-Rolling of Dual-Phase Zirconium Alloys, The University of Manchester, 2018.

[26] A. Godfrey, O. V. Mishin, T. Yu, Characterization and influence of deformation microstructure heterogeneity on recrystallization, IOP Conf. Ser. Mater. Sci. Eng. 89 (2015) 012003. doi:10.1088/1757-899X/89/1/012003.

[27] H.E. Rosinger, D.O. Northwood, The elastic properties of zirconium fuel cladding and pressure tubing materials, J. Nucl. Mater. 79 (1979) 170–179.

[28] J. Gong, T. Benjamin Britton, M.A. Cuddihy, F.P.E. Dunne, A.J. Wilkinson, ⟨a⟩ Prismatic, ⟨a⟩ basal, and ⟨c+a⟩ slip strengths of commercially pure Zr by micro-cantilever tests, Acta Mater. 96 (2015) 249–257. doi:10.1016/j.actamat.2015.06.020.

[29] N. Gey, M. Humbert, M.J. Philippe, Y. Combres, Modeling the transformation texture of Ti-64 sheets after rolling in the β-field, Mater. Sci. Eng. A. 230 (1997) 68–74. doi:10.1016/S0921-5093(97)80111-6.

[30] H. Moustahfid, M. Humbert, M.J. Philippe, Modeling of the texture transformation in a Ti-64 sheet after hot compression, Acta Mater. 45 (1997) 3785–3790. doi:10.1016/S1359-6454(97)00038-4.

[31] M.R. Daymond, R.A. Holt, S. Cai, P. Mosbrucker, S.C. Vogel, Texture inheritance and variant selection through an hcp–bcc–hcp phase transformation, Acta Mater. 58 (2010) 4053–4066. doi:10.1016/j.actamat.2010.03.012.

[32] D. Bhattacharyya, G.. Viswanathan, R. Denkenberger, D. Furrer, H.L. Fraser, The role of crystallographic and geometrical relationships between α and β phases in an α/β titanium alloy, Acta Mater. 51 (2003) 4679–4691. doi:10.1016/S1359-6454(03)00179-4.

[33] R. Shi, V. Dixit, H.L. Fraser, Y. Wang, Variant selection of grain boundary α by special prior β grain boundaries in titanium alloys, Acta Mater. 75 (2014) 156–166. doi:10.1016/j.actamat.2014.05.003.

[34] R.E. Logé, J.W. Signorelli, Y.B. Chastel, M.Y. Perrin, R.A. Lebensohn, Sensitivity of α-Zy4 high-temperature deformation textures to the β-quenched precipitate structure and to recrystallization: application to hot extrusion, Acta Mater. 48 (2000) 3917–3930. doi:10.1016/S1359-6454(00)00179-8.

[35] D.G. Leo Prakash, M. Preuss, M. Dahlbäck, J. Quinta da Fonseca, Microstructure and texture evolution during thermomechanical processing of β-quenched Zr, Acta Mater. 88 (2015) 389–401. doi:10.1016/j.actamat.2014.12.033.

[36] S.L. Semiatin, An Overview of the Thermomechanical Processing of α/β Titanium Alloys: Current Status and Future Research Opportunities, Metall. Mater. Trans. A. (2020) 1–102. doi:10.1007/s11661-020-05625-3.

[37] D.G.L. Prakash, R. Ding, R.J. Moat, I. Jones, P.J. Withers, J.Q. da Fonseca, M. Preuss, Deformation twinning in Ti-6Al-4V during low strain rate deformation to moderate strains at room temperature, Mater. Sci. Eng. A. 527 (2010) 5734–5744. doi:10.1016/j.msea.2010.05.039.

[38] G.C. Obasi, S. Birosca, D.G. Leo Prakash, J. Quinta da Fonseca, M. Preuss, The influence of

rolling temperature on texture evolution and variant selection during α→β→α phase transformation in Ti–6Al–4V, Acta Mater. 60 (2012) 6013–6024. doi:10.1016/j.actamat.2012.07.025.

[39] S. Cai, M.R. Daymond, R.A. Holt, M.A. Gharghouri, E.C. Oliver, Evolution of interphase and intergranular stresses in Zr–2.5Nb during room temperature deformation, Mater. Sci. Eng. A. 501 (2009) 166–181. doi:10.1016/j.msea.2008.10.016.

[40] S. Cai, M.R. Daymond, R.A. Holt, Deformation of high β-phase fraction Zr–Nb alloys at room temperature, Acta Mater. 60 (2012) 3355–3369. doi:10.1016/j.actamat.2012.02.040.

[41] J.J. Jonas, C. Ghosh, Role of mechanical activation in the dynamic transformation of austenite, Acta Mater. 61 (2013) 6125–6131. doi:10.1016/j.actamat.2013.06.054.

[42] R. Ding, Z.X. Guo, A. Wilson, Microstructural evolution of a Ti–6Al–4V alloy during thermomechanical processing, Mater. Sci. Eng. A. 327 (2002) 233–245. doi:10.1016/S0921-5093(01)01531-3.

[43] B. Guo, C. Aranas, B. Sun, X. Ji, J.J. Jonas, Reverse Transformation Behavior of Ti-6Al-4V After Deformation in the Two-Phase Region, Metall. Mater. Trans. A Phys. Metall. Mater. Sci. 49 (2018) 22–27. doi:10.1007/s11661-017-4403-4.

[44] B. Guo, S.L. Semiatin, J. Liang, B. Sun, J.J. Jonas, Opposing and Driving Forces Associated with the Dynamic Transformation of Ti-6Al-4V, Metall. Mater. Trans. A Phys. Metall. Mater. Sci. 49 (2018) 1–5. doi:10.1007/s11661-018-4551-1.

[45] R.A. Holt, P. Zhao, Micro-texture of extruded Zr–2.5Nb tubes, J. Nucl. Mater. 335 (2004) 520–528. doi:10.1016/j.jnucmat.2004.07.043.

[46] M. Humbert, N. Gey, Elasticity-based model of the variant selection observed in the β to α phase transformation of a Zircalloy-4 sample, Acta Mater. 51 (2003) 4783–4790. doi:10.1016/S1359-6454(03)00318-5.

[47] P.D. Honniball, M. Preuss, D. Rugg, J. Quinta da Fonseca, Grain Breakup During Elevated Temperature Deformation of an HCP Metal, Metall. Mater. Trans. A. 46 (2015) 2143–2156. doi:10.1007/s11661-015-2812-9.

[48] F. Wagner, N. Bozzolo, O. Van Landuyt, T. Grosdidier, Evolution of recrystallisation texture and microstructure in low alloyed titanium sheets, Acta Mater. 50 (2002) 1245–1259. doi:10.1016/S1359-6454(01)00427-X.

[49] D.A. Porter, K.E. Easterling, M.Y. Sherif, Phase Transformations in Metals and Alloys, 3rd ed., CRC Press, Taylor & Francis Group, Boca Raton, Florida, 2009.

[50] M.K. Kumar, I. Samajdar, N. Venkatramani, G.K. Dey, R. Tewari, D. Srivastava, S. Banerjee, Explaining absence of texture development in cold rolled two-phase Zr–2.5 wt% Nb alloy, Acta Mater. 51 (2003) 625–640. doi:10.1016/S1359-6454(02)00442-1.

[51] P.S. Bate, J. Quinta da Fonseca, Texture development in the cold rolling of IF steel, Mater. Sci. Eng. A. 380 (2004) 365–377. doi:10.1016/j.msea.2004.04.007.

[52] A. Després, M. Zecevic, R.A. Lebensohn, J.D. Mithieux, F. Chassagne, C.W. Sinclair, Contribution of intragranular misorientations to the cold rolling textures of ferritic stainless steels, Acta Mater. 182 (2020) 184–196. doi:10.1016/j.actamat.2019.10.023.

[53] L. Kestens, S. Jacobs, Texture Control During the Manufacturing of Nonoriented Electrical Steels, Texture, Stress. Microstruct. (2008) 1–9. doi:10.1155/2008/173083.

[54] N. Gey, M. Humbert, M.J. Philippe, Y. Combres, Investigation of the α- and β- texture evolution of hot rolled Ti-64 products, Mater. Sci. Eng. A. 219 (1996) 80–88. doi:10.1016/S0921-5093(96)10388-9.

[55] C. Nguyen, M. Balzer, T. Witulski, M. Böhm, B. Dod, M. Preuss, J. Quinta, Understanding the β-phase texture development in Ti-6Al-4V during compression in the α + β regimes, in: 14th World Conf. Titan., MATEC Web of Conferences, Nantes, France, 2019. doi:10.5281/zenodo.3381205.

[56] S. Roy, R. Madhavan, S. Suwas, Crystallographic texture and microstructure evolution during hot compression of Ti–6Al–4V–0.1B alloy in the (α + β)-regime, Philos. Mag. 94 (2014) 358–380. doi:10.1080/14786435.2013.853141.

[57] H. Moustahfid, N. Gey, M. Humbert, M.J. Philippe, Study of the β-α phase transformations of a Ti-64 sheet induced from a high-temperature β state and a high-temperature α + β state, Metall. Mater. Trans. A. 28 (1997) 51–61. doi:10.1007/s11661-997-0082-x.

[58] R. Shi, Y. Wang, Variant selection during α precipitation in Ti–6Al–4V under the influence of local stress – A simulation study, Acta Mater. 61 (2013) 6006–6024. doi:10.1016/j.actamat.2013.06.042.

[59] R. Shi, V. Dixit, H.L. Fraser, Y. Wang, Variant selection of grain boundary α by special prior β grain boundaries in titanium alloys, Acta Mater. 75 (2014) 156–166. doi:10.1016/j.actamat.2014.05.003.

[60] C.S. Daniel, C.-T. Nguyen, M.D. Atkinson, J. Quinta da Fonseca, Direct Evidence for a Dynamic Phase Transformation during High Temperature Deformation in Ti-64 [Preprint], in: 14th World Conf. Titan., MATEC Web of Conferences, Nantes, France, 2019. doi:10.5281/zenodo.3381183.

[61] D.G. Leo Prakash, P. Honniball, D. Rugg, P.J. Withers, J. Quinta da Fonseca, M. Preuss, The effect of β phase on microstructure and texture evolution during thermomechanical processing of α+β Ti alloy, Acta Mater. 61 (2013) 3200–3213. doi:10.1016/j.actamat.2013.02.008.

[62] L. Germain, N. Gey, M. Humbert, P. Bocher, M. Jahazi, Analysis of sharp microtexture

heterogeneities in a bimodal IMI 834 billet, Acta Mater. 53 (2005) 3535–3543. doi:10.1016/j.actamat.2005.03.043.

[63] M. Humbert, L. Germain, N. Gey, P. Bocher, M. Jahazi, Study of the variant selection in sharp textured regions of bimodal IMI 834 billet, Mater. Sci. Eng. A. 430 (2006) 157–164. doi:10.1016/j.msea.2006.05.047.

[64] I. Bantounas, D. Dye, T.C. Lindley, The role of microtexture on the faceted fracture morphology in Ti–6Al–4V subjected to high-cycle fatigue, Acta Mater. 58 (2010) 3908–3918. doi:10.1016/j.actamat.2010.03.036.

[65] K. Zhang, K.V. Yang, S. Lim, X. Wu, C.H.J. Davies, Effect of the presence of macrozones on short crack propagation in forged two-phase titanium alloys, Int. J. Fatigue. 104 (2017) 1–11. doi:10.1016/j.ijfatigue.2017.07.002.

[66] T.R. Bieler, S.L. Semiatin, The origins of heterogeneous deformation during primary hot working of Ti–6Al–4V, Int. J. Plast. 18 (2002) 1165–1189. doi:10.1016/S0749-6419(01)00057-2.

[67] S. Roy, R. Madhavan, S. Suwas, Crystallographic texture and microstructure evolution during hot compression of Ti–6Al–4V–0.1B alloy in the (α + β)-regime, Philos. Mag. 94 (2014) 358–380. doi:10.1080/14786435.2013.853141.

Figures

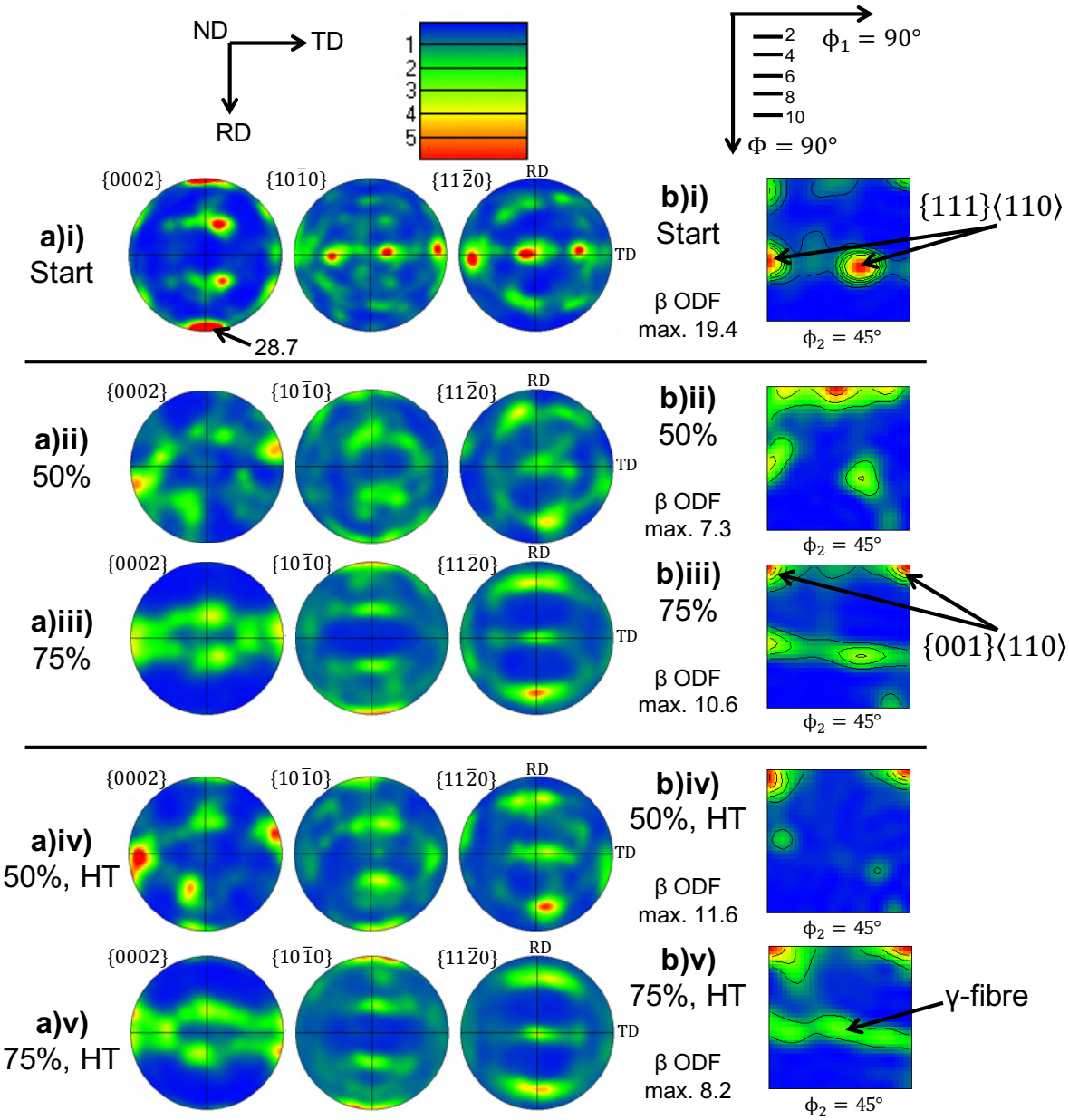

Figure 1: α and β phase texture development in the Zircaloy-4 + 7 wt.% Nb alloy, showing evolution of (i) starting orientations, after rolling at 725°C to reductions of (ii) 50% reduction, (iii) 75% reduction, (iv) 50% reduction with annealing heat-treatment (HT) and (v) 75% reduction with annealing HT. The α-phase {0002}, {10$\bar{1}$0} and {11$\bar{2}$0} pole figures (a) show a starting transformation texture, with basal poles strongly aligned in RD, which during hot-rolling develops a very different {11$\bar{2}$0}⟨10$\bar{1}$0⟩ transverse texture component, aligning 0002||TD. The β-phase ODF slice at $\phi_2 = 45°$ (a) show a strong initial {111}⟨110⟩ component, which breaks up into a γ-fibre and {001}⟨110⟩ rotated cube orientations.

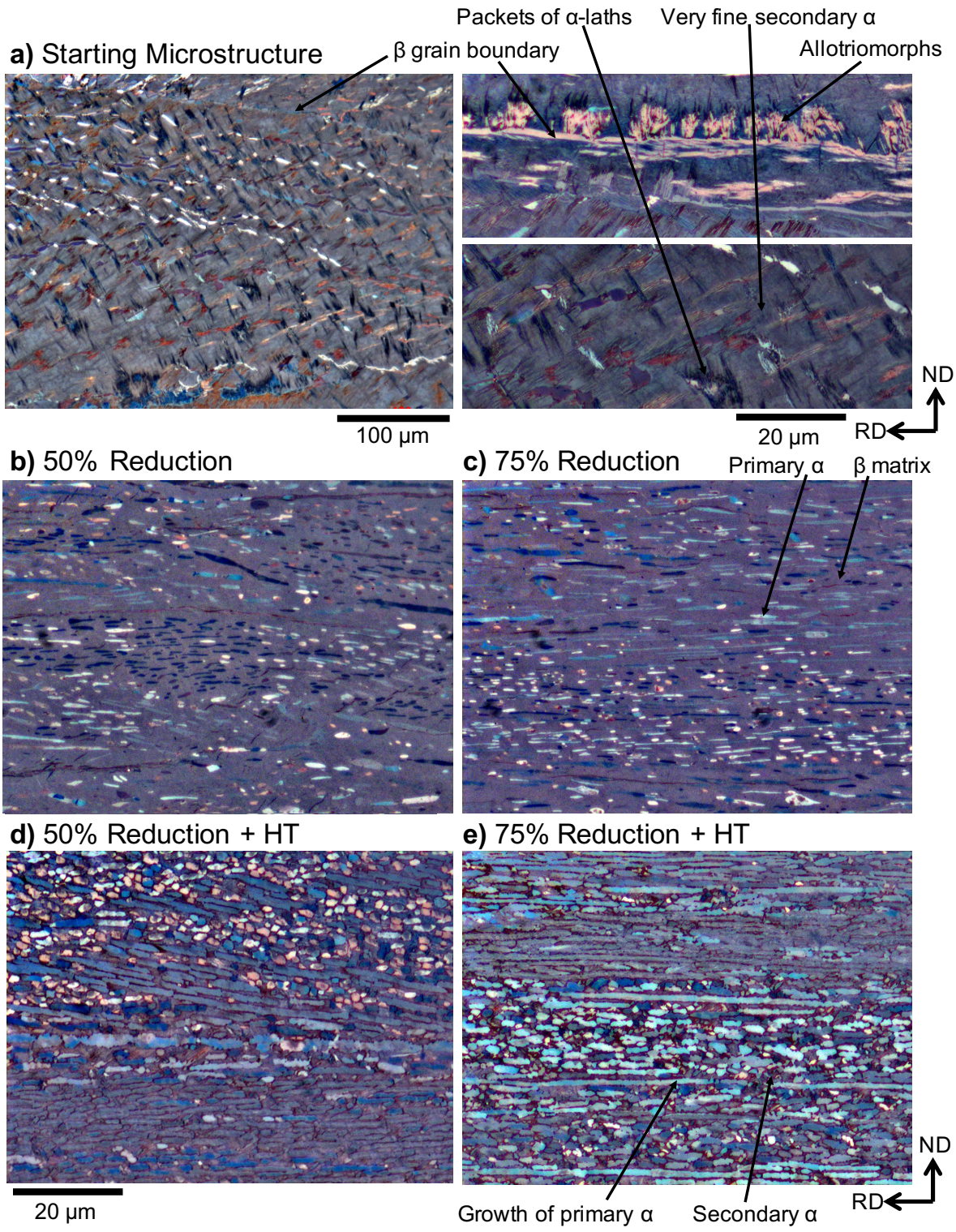

Figure 2: Optical polarised light micrographs of the starting and rolled Zircaloy-4 + 7 wt.% Nb material. The starting microstructure (a) shows packets of α-laths, with some very fine secondary α-laths within the β-matrix, and a few elongated α lamellae formed along β grain boundaries. The rolled microstructures in (b) at 50% reduction and (c) at 75% reduction are taken in the RD-ND plane (TD direction), showing elongated primary α grains within the β-matrix. The annealed microstructures in (d) and (e) show growth of the primary α, with some secondary α precipitation.

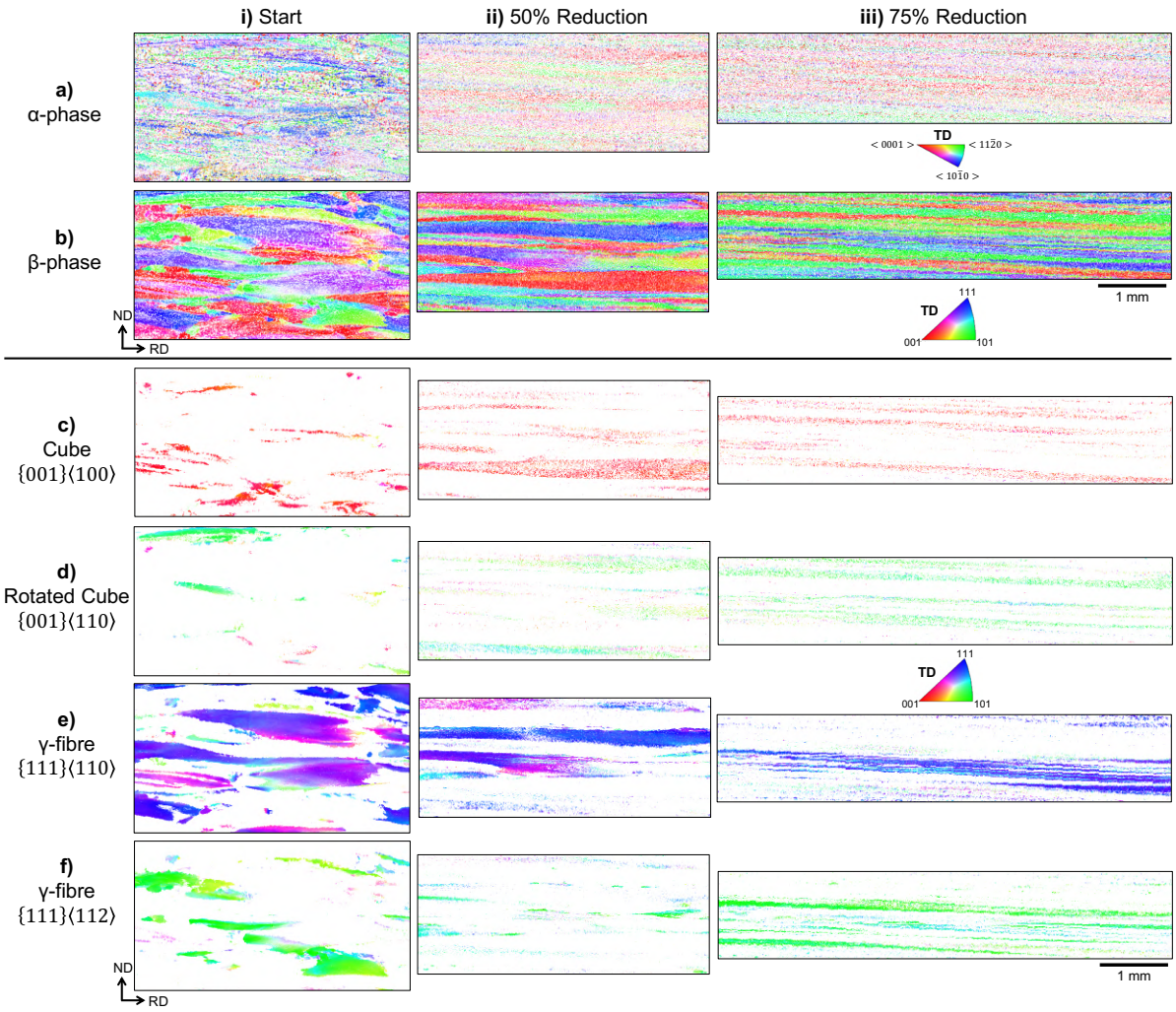

Figure 3: EBSD orientation maps, showing (a) indexed α orientations and (b) indexed β orientations in the (i) the starting material and after rolling to (ii) 50% reduction and (iii) 75% reduction. The EBSD slices are taken with respect to the rolling directions, in the RD-ND plane (TD direction) and with IPF colouring in TD. Different β-grains have been isolated, with texture components forming the (a) {001}⟨100⟩ cube, (b) {001}⟨110⟩ rotated cube (c) {111}⟨110⟩ γ-fibre and (d) {111}⟨112⟩ γ-fibre orientation, to show the extent of breakup at the different stages.

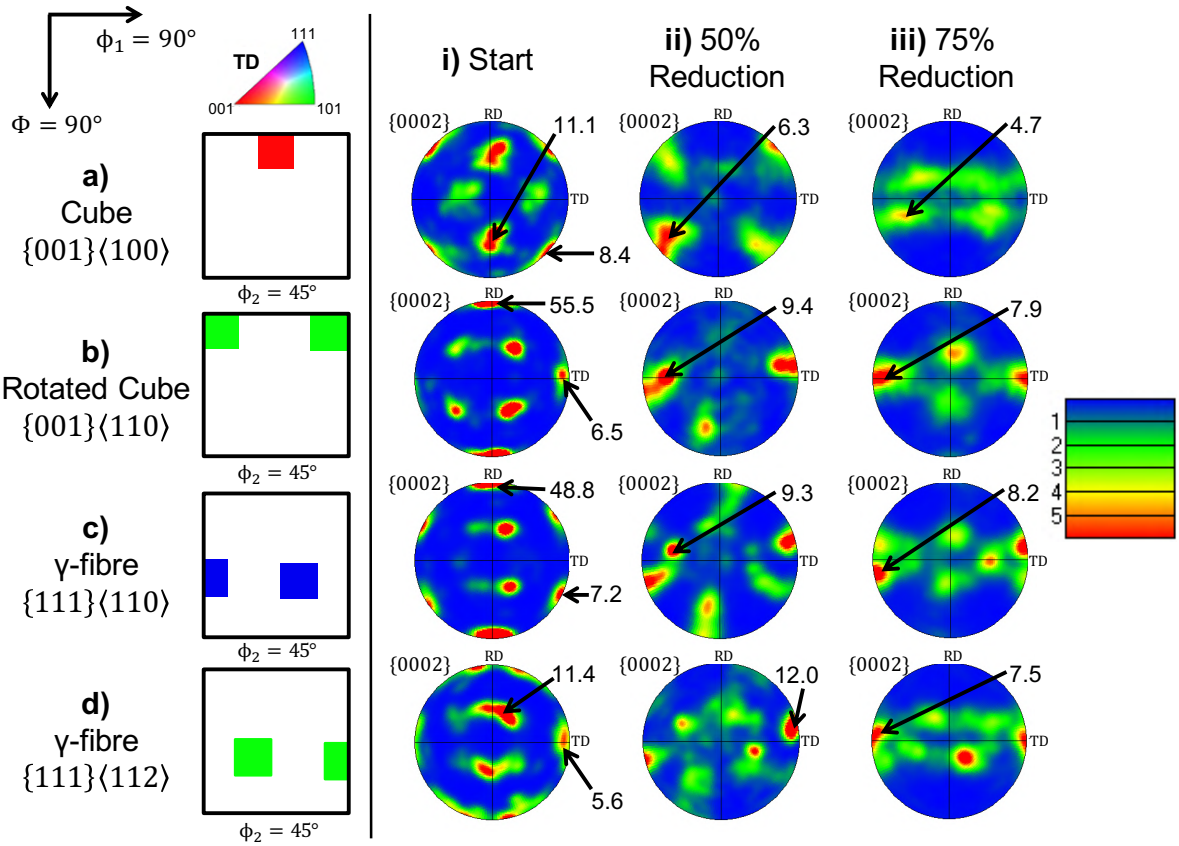

Figure 4: α-phase {0002} pole figures measured from differently orientated β-grains. Showing the α orientations contained within β-grains with (a) {001}⟨100⟩ cube, (b) {001}⟨110⟩ rotated cube (c) {111}⟨110⟩ γ-fibre and (d) {111}⟨112⟩ γ-fibre texture components, taken from material at the start (i) and after rolling to (ii) 50% and (iii) 75% reduction. After just 50% reduction, any 0002||RD or 0002||ND variants preferentially dissolve, which coincides with a strengthening of the 0002||TD.

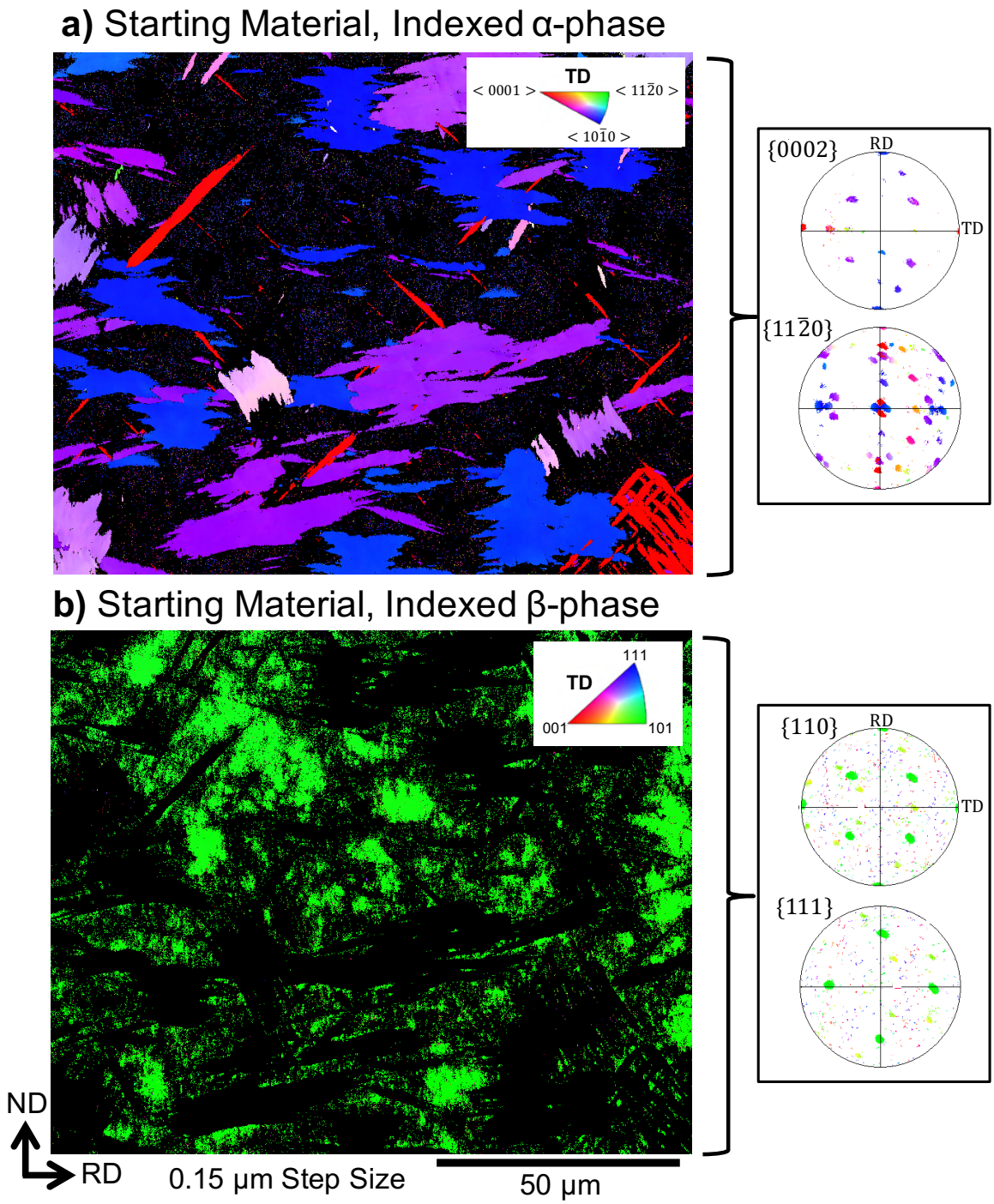

Figure 5: Fine EBSD orientation maps of the starting material, showing (a) indexed α-grains and (b) indexed β orientations, both with IPF colouring in TD. The different orientations of α-lath packets, as shown by the associated α $\{0002\}$ and $\{11\bar{2}0\}$ pole figures in (a), match the Burgers relationship with the surrounding β-grain, with orientation shown by the β $\{110\}$ and $\{111\}$ pole figures in (b).

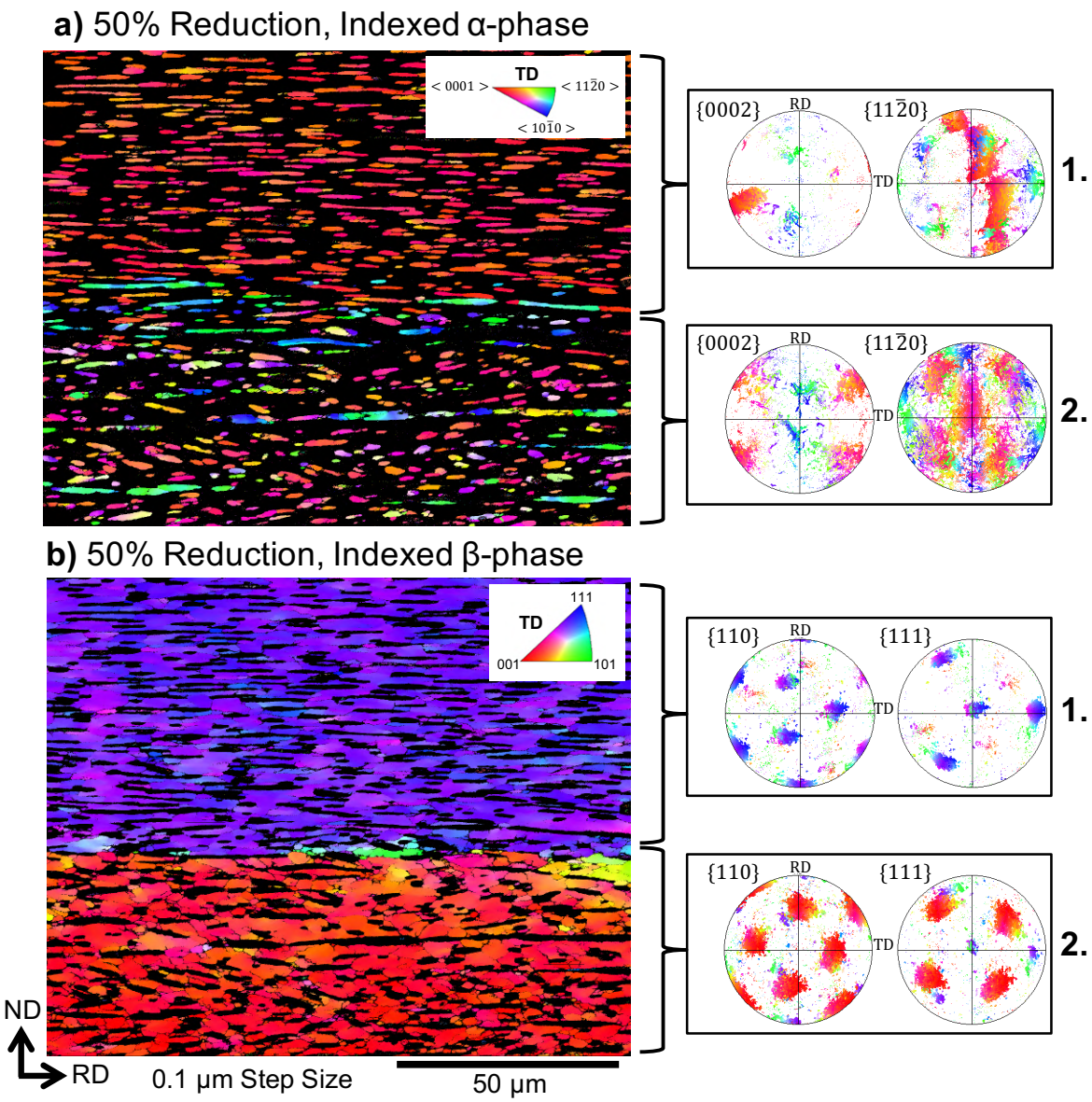

Figure 6: Orientation maps taken after rolling to 50% reduction, indexing (a) the α-grains and (b) the β orientations, both with IPF colouring in TD. There is some agreement with the Burgers relationship in the two different β-grains (labelled 1 and 2), shown by comparing the associated α {0002} and {11$\bar{2}$0} pole figures in (a) and the β {110} and {111} pole figures in (b). However, there is only one primary α variant left, with 0002||TD, in region 1.

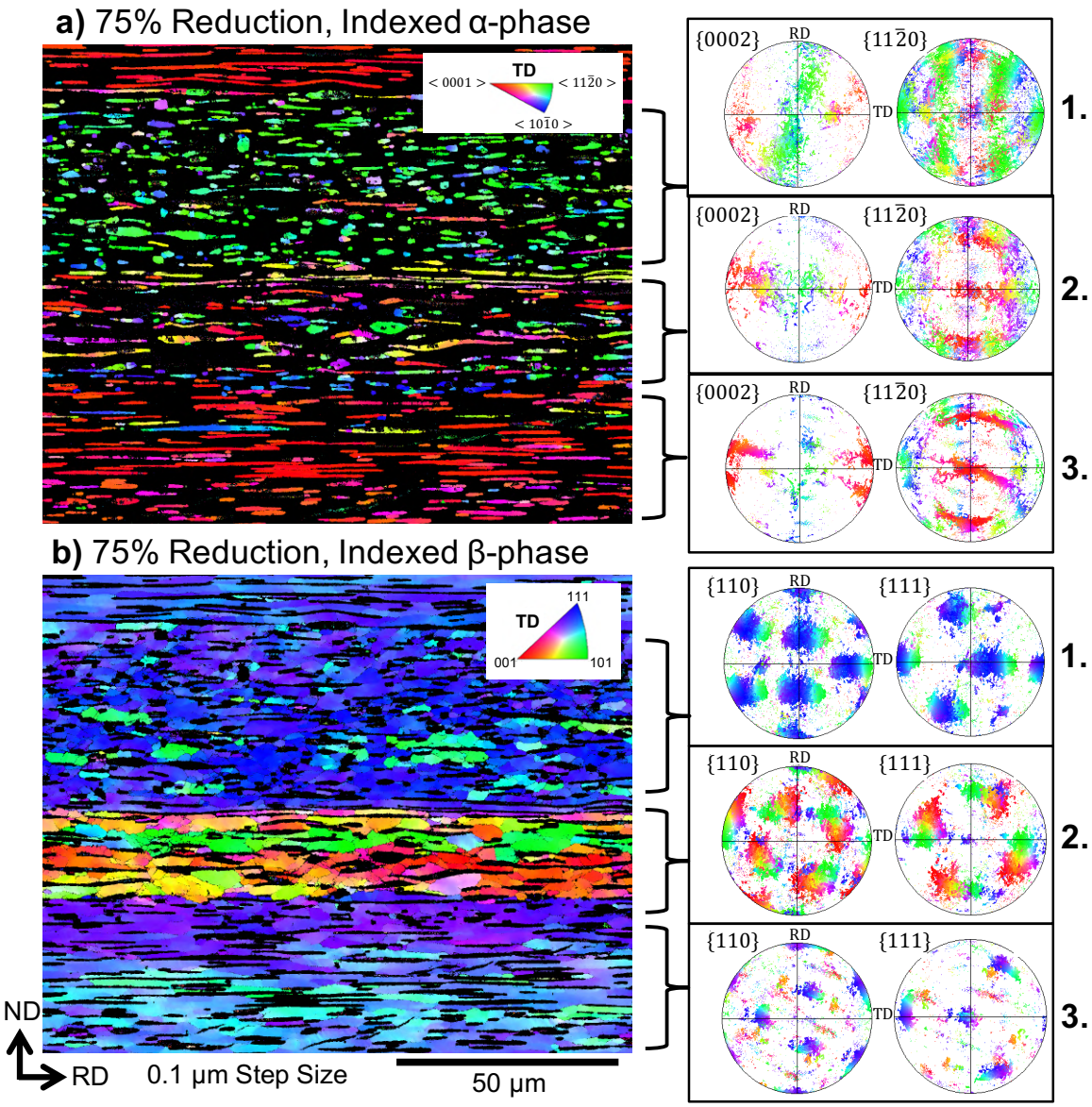

Figure 7: Orientation maps taken after rolling to 75% reduction, showing (a) indexed α-grains and (b) indexed β orientations. The α {0002} and {11$\bar{2}$0} pole figures in (a) and β {110} and {111} pole figures in (b) are shown for three different β-grains (labelled 1, 2 and 3). The crystallographic orientation of the primary α grains influences the misorientation in the surrounding β-matrix, shown by the spread in the pole figures. The misorientation is lowest for grains with 0002||TD. There is also no longer a clear agreement with the Burgers relationship.

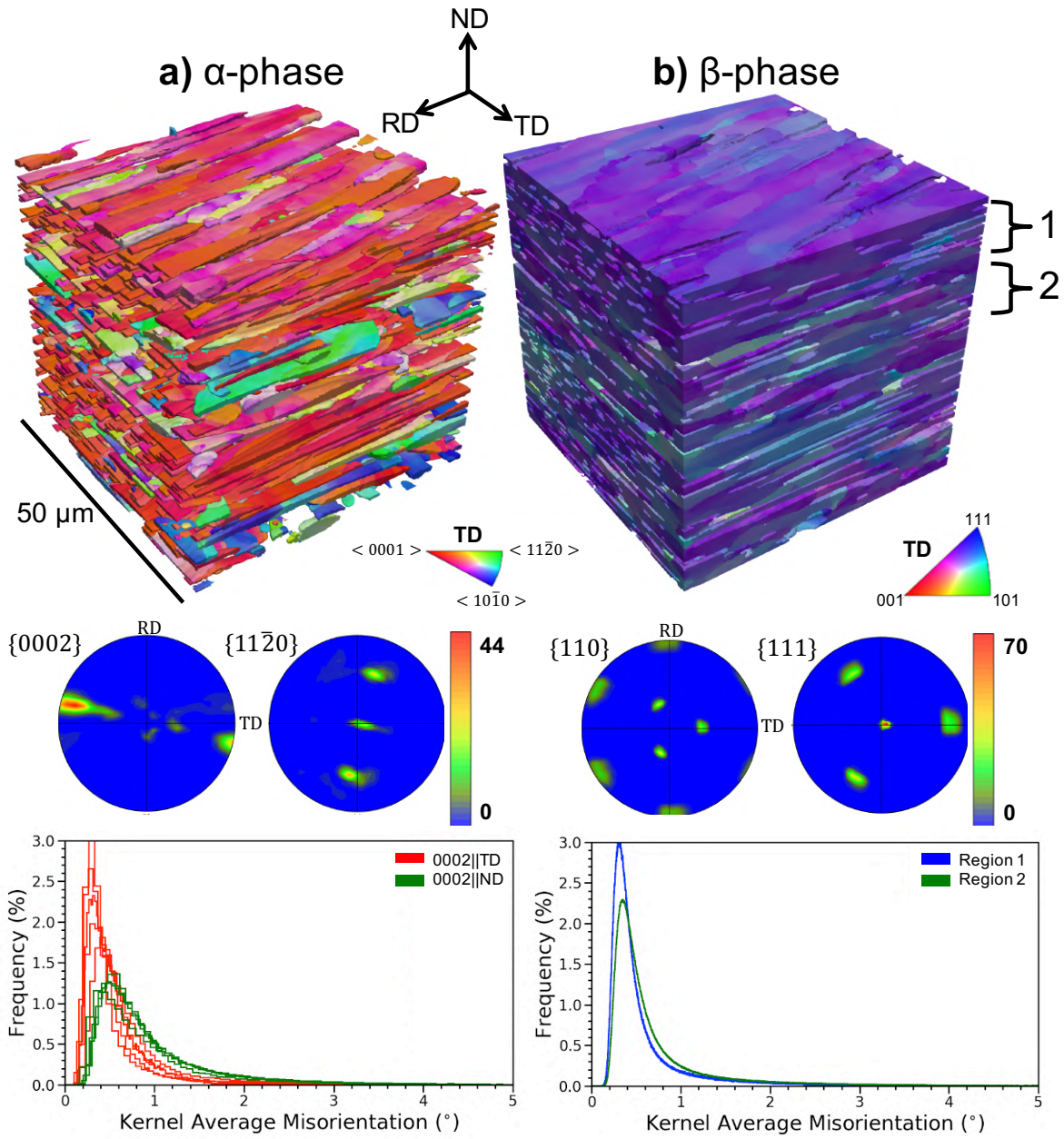

Figure 8: 3D EBSD reconstruction of the Zircaloy-4 + 7 wt.% Nb alloy rolled to 75% reduction, showing (a) the retained primary α grains and (b) the retained β-matrix, both with IPF colouring in TD. The α-phase shows a favoured transverse texture component with ⟨0002⟩ aligned slightly off-axis from TD in the pole figure, as well as the β-phase showing a strong {111}⟨110⟩ γ-fibre component. The α-phase kernel average misorientation (KAM) distribution for grains with a main 0002||TD orientation is lower compared with grains with 0002||ND. The KAM distribution for the β-phase also show similar differences for regions of the β-grain surrounding mostly α-grains with 0002||TD (region 1) and 0002||ND grains (region 2).

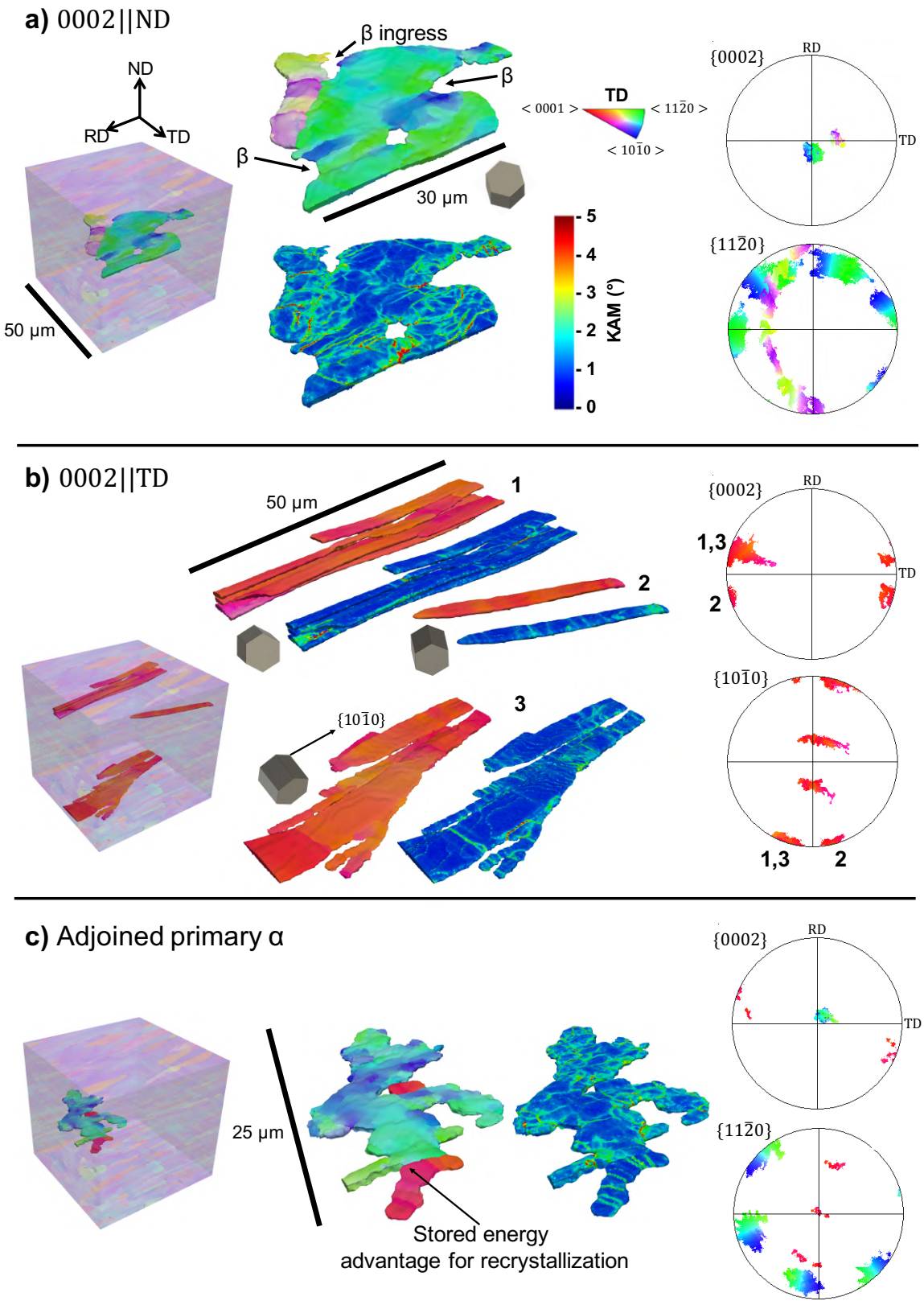

Figure 9: Individual primary α grains selected from the 3D EBSD reconstruction, showing the grain morphology and misorientation spread for different crystallographic orientations. In (a) two flat plates form with 0002||ND, which develops a relatively high misorientation across the grain and a large orientation spread throughout the pole figure. In (b) two small attached plates with 0002||TD have a stored energy advantage to consume one grain orientated with 0002||ND, via recrystallization or phase transformation. In (c) three α-grains (1, 2, 3) with 0002||TD form highly

elongated flat plate lamellae, each with a stable transverse texture component and crystallographic alignment of the $\langle 10\bar{1}0 \rangle$ with the long axis.